Journal of Materials Physics and Chemistry, 2024, Vol. 12, No. 1, 17-21
Available online at http://pubs.sciepub.com/jmpc/12/1/3
Published by Science and Education Publishing
DOI:10.12691/jmpc-12-1-3

Magnetostatic Modeling and Thermal Losses Estimation in a Nickel-based Curie Wheel

Serge Dzo Mawuefa Afenyiveh[1,*], Assiongbon Adanlété Adjanoh[1], Tchilabalo Pakam[1], Yogoubé Goudo[1,2], Mohamadou Tchakpi[1,2], Akiza Bidjagare[1], Katchegbélé Yawovi Kable[1], Bila Gnoate Yenteme[1,2]

[1]Laboratoire Materiaux, Energies Renouvelables et Environnement, Physics Department, Université de Kara, Kara, Togo
[2]Laboratoire de Physique des Matériaux et des Composants à Semi-conducteurs, Physics Department, Université de Lomé, Lomé, Togo
*Corresponding author: dzo.serge@gmail.com

Received February 10, 2024; Revised March 12, 2024; Accepted March 19, 2024

Abstract This article introduces a method to evaluate the magnetic interaction between permanent magnets and active materials, comprised of nickel pellets, within a Curie wheel. Additionally, an approach to estimate thermal losses is presented to control heat dissipation, thereby mitigating heat accumulation in the active material.

Keywords: *curie wheel, magnetic model, heat losses*

Cite This Article: Serge Dzo Mawuefa Afenyiveh, Assiongbon Adanlété Adjanoh, Tchilabalo Pakam, Yogoubé Goudo, Mohamadou Tchakpi, Akiza Bidjagare, Katchegbélé Yawovi Kable, and Bila Gnoate Yenteme, "Magnetostatic Modeling and Thermal Losses Estimation in a Nickel-based Curie Wheel." *Journal of Materials Physics and Chemistry*, vol. 12, no. 1 (2024): 17-21. doi: 10.12691/jmpc-12-1-3.

1. Introduction

Curie motors offer an interesting approach to converting heat into mechanical work by exploiting the thermomagnetic coupling phenomenon. This coupling, which involves the interaction between magnetic field and temperature gradient, presents promising opportunities for the development of sustainable power generation solutions [1,2,3,4,5]. The efficiency of thermomagnetic motors is subject to the influence of various factors, including the mechanical design of the system. The thermomagnetic properties of permanent magnets, encompassing coercivity (H_C), remanence (B_r), and Curie temperature (T_C), play a central role in these dynamics. The structural, thermophysical, and magnetic characteristics of the active material, as well as the absorbed thermal energy, play a significant role in shaping the overall performance of the motor [6]. These interconnected factors collectively contribute to shaping the motor's efficiency, highlighting the multidimensional nature of thermomagnetic system optimization. In a recent work [6], we've presented a thermal simulation of a Curie motor, considering various configurations. In this study, we first, present magnetic modelling for understanding the mechanical aspects of the system and also thermal losses analysis to control heat accumulation on active materials. The ultimate goal of our research is to contribute to the advancement of Curie motor technologies by offering insights into the design, optimization, and practical implementation of thermomagnetic power generation systems. Nickel (Ni), due to its distinctive characteristics, holds a crucial position in the composition of magnetic materials. Apart from economic considerations, it is chosen as the active material for several reasons. Among commonly used ferromagnetic materials available at reasonable cost, such as iron (Fe) and cobalt (Co), Ni stands out with its relatively low magnetic transition temperature, denoted as T_C^{Ni} = 631 K, compared to that of Fe (T_C^{Fe} = 1043 K) and Co (T_C^{Co} = 1394 K).

Ni, used as active material, is the central element of this study due to its availability and unique magnetic properties. A shiny white metal, relatively hard, malleable, and ductile, it exhibits a density of 8.90 g/cm³ at 20°C and a melting point of 1453°C. Crystallizing in a face-centered cubic structure, Ni is ferromagnetic until 355°C, its Curie point, with magnetism primarily attributed to its electron configuration $3d^8 4s^2$, typical of transition metals.

2. Operating Principle of the Device

The device as shown in Figure 1 operates based on the Curie wheel, positioned horizontally near the heat source. It is equipped with Ni pellets as active materials, arranged on the lateral surface of the disk. A magnetic pole composed of Neodymium-Iron-Boron (NdFeB) magnets is held on the periphery of the wheel.

The thermomagnetic device utilizes the permanent magnet to generate a uniform and uniaxial magnetic field $\vec{M}$. This field induces an attractive force on the active material positioned on the disk. The active materials are strategically placed equidistantly in front of the permanent magnet, along the circumference of the equilibrium wheel.

Asymmetry arises when the active material is heated

beyond its Curie temperature on one side of the magnet. Upon reaching this temperature, the active material undergoes a phase transition from the ferromagnetic to the paramagnetic state. Magnetization is much stronger in the former phase, causing an imbalance of forces on either side of the wheel, prompting it to rotate as the force exerted by the magnet on the ferromagnetic part is significantly greater than that applied to the paramagnetic part.

The light source used is the sun, chosen for its availability. A parabolic solar concentrator focuses solar rays onto the active material.

To prevent heat buildup, an aluminum (Al) layer is simulated in our previous works [6] as a radiator, facilitating device cooling.

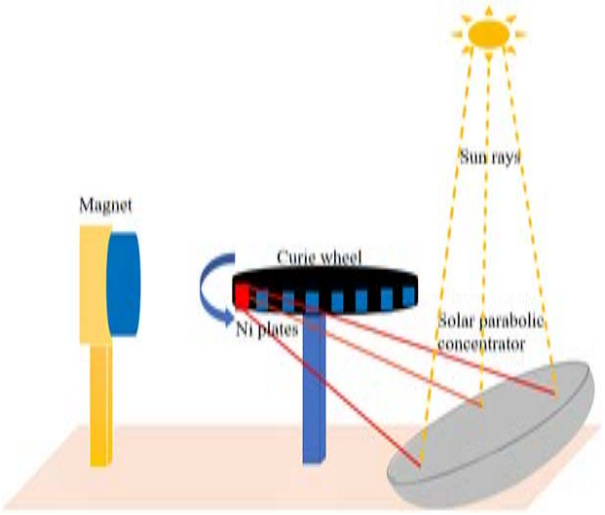

Figure 1. Curie Device configuration[4]

3. Magnetic Modeling

3.1. Magnetic Field Created by the Magnet on the Plate

Several works have proposed analytical models following the geometry of the permanent magnet (PM), for magnetic simulation [7,8,9,10,11,12]. According to Furlani [12] and assuming that the active material is uniformly magnetized with a uniaxial magnetization along the x-axis of space, the magnetic flux density (B_{PM}) created by the PM on the active material (AM) is expressed by:

$$B_{PM}(x) = \frac{\mu_0 M_s}{\pi}\left[\tan^{-1}\tan^{-1}\left(\frac{(x+th_{PM})\sqrt{l^2+w^2+(x+th_{PM})^2}}{l*w}\right) - \tan^{-1}\tan^{-1}\left(\frac{x*\sqrt{l^2+w^2+x^2}}{l*w}\right)\right] \quad (1)$$

where $\mu_0 M_s = B_r$ is the remanent flux density of the magnetic source, $\mu_0 = 4\pi \times 10^{-7}\ A/m$ is the permeability of vacuum, and M_S is the saturation magnetization. *x*, th_{PM}, *2l*, and *2w* are respectively the distance permanent magnet – active material, the thickness of the magnet, its length, and its width.

3.2. Mechanical Approach of the Curie Wheel

The demagnetizing field plays a very important role in the magnetization process. In a linear, homogeneous, and isotropic medium, magnetization $\vec{M}$ is linearly proportional to the magnetic excitation $\vec{M}$ by the relationship [13]:

$$\vec{M} = \chi\vec{H} \quad (2)$$

where χ is the magnetic susceptibility of the material defined by the Curie-Weiss equation:

$$\chi = \frac{C}{T} \quad (3)$$

C is the Curie-Weiss constant, and T is the temperature of the magnetic material.

In equation (3), the magnetic field $\vec{M}$ represents the total field, which is the superposition of the applied magnetic field $\vec{H}_0$ (responsible for the magnetization of the magnetic material) and the demagnetizing field $\vec{H}_d$ (discovered by P. Weiss [14] in pyrrhotite) created by magnetization. Thus, we have:

$$\vec{H} = \vec{H}_0 + \vec{H}_d \quad (4)$$

Where

$$\vec{H}_d = -d * \vec{M} \quad (5)$$

The demagnetizing factor has components that are linear combinations of the magnetization components $\vec{M}$:

$$d = \begin{pmatrix} d(x) & 0 & 0 \\ 0 & d(y) & 0 \\ 0 & 0 & d(z) \end{pmatrix} \quad (6)$$

where

$$d(x)+d(y)+d(z)=1 \quad (7)$$

Estimating demagnetizing factors is necessary for accurately determining true remanent magnetization, especially in the numerical resolution of magnetic application problems.

There are several analytical methods for determining the demagnetizing factor [15,16,17]. Considering a uniform and homogeneous ferromagnetic material in the form of a rectangular prism, A. Aharoni [17] proposes a model for calculating the demagnetizing factor in the thickness direction (z-axis) according to:

The other two demagnetizing factors $d(x)$ and $d(y)$ can be derived from this equation by performing a double cyclical permutation of the orientation of its position.

The magnetic force depends on the magnetization $\vec{M}$ and the magnetic excitation $\vec{M}$. Therefore, it is necessary to estimate the demagnetizing field $\vec{H}_d$ from the demagnetizing factor d.

$$d(z)=\frac{1}{\pi}\left[\begin{array}{l}\frac{c}{2a}ln\left(\frac{\sqrt{b^2+c^2}-b}{\sqrt{b^2+c^2}+b}\right)+\frac{c}{2b}ln\left(\frac{\sqrt{a^2+c^2}-a}{\sqrt{a^2+c^2}+a}\right)\\+\frac{a}{2c}ln\left(\frac{\sqrt{a^2+b^2}+b}{\sqrt{a^2+b^2}-b}\right)+\frac{b}{2c}ln\left(\frac{\sqrt{a^2+b^2}+a}{\sqrt{a^2+b^2}-a}\right)\\+\frac{c}{ab}\left(\sqrt{a^2+c^2}+\sqrt{b^2+c^2}\right)+\frac{\left(a^2-c^2\right)}{2ac}ln\left(\frac{\sqrt{a^2+b^2+c^2}-b}{\sqrt{a^2+b^2+c^2}+b}\right)\\+\frac{\left(b^2-c^2\right)}{2bc}ln\left(\frac{\sqrt{a^2+b^2+c^2}-a}{\sqrt{a^2+b^2+c^2}+a}\right)+\frac{a^3+b^3-2c^3}{3abc}\\+\frac{\left(a^2+b^2-2c^2\right)}{3abc}\sqrt{a^2+b^2+c^2}+\frac{\left(a^2+b^2\right)^{\frac{3}{2}}+\left(a^2+c^2\right)^{\frac{3}{2}}}{3abc}\\+2tan^{-1}\left(\frac{ab}{c\sqrt{a^2+b^2+c^2}}\right)\end{array}\right] \quad (8)$$

The permanent magnet (PM) and the active material (AM) are respectively characterized by their magnetic charges Q_{PM} and Q_{AM}. According to the dipole model, the magnetic force is given by the relation:

$$F=\frac{\mu_0}{4\pi r^2}Q_{PM}*Q_{AM} \quad (9)$$

The charge density and magnetization can be defined by the equations

$$Q=MS \quad (10)$$

where S is the surface of the active material, and

$$M=\frac{B_0}{\mu_0 d} \quad (11)$$

where B_0 is the applied field and d is the demagnetizing factor. This gives

$$Q=\frac{B_0}{\mu_0}*\frac{S}{d} \quad (12)$$

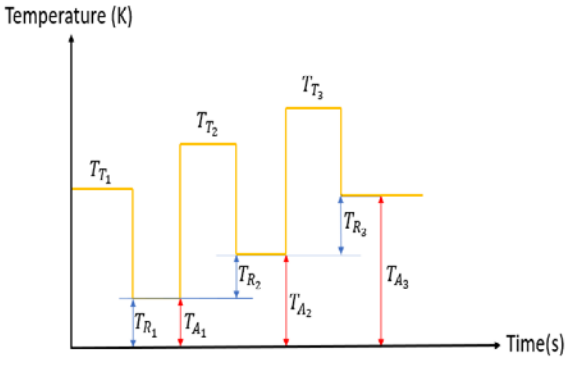

Figure 2. Dynamic behaviour of the active material

4. Quantification of Thermal Losses

One of the major challenges in the design of thermomagnetic heat conversion systems is the accumulation of heat in the active material as shown in Figure 2, and defined by the relation [18]:

$$T_{Ai}=T_i+\sum_{i=1}^{n}T_{Ri} \quad (13)$$

With T_i, T_{Ri} and T_{Ai} being respectively the initial, the residual and the accumulated temperature during n-cycle of heating and cooling.

4.1. Expression of the time Constant of Temperature for a Rotation Without Thermal Loss

Here, we will estimate the expression of the temperature dependence over time by neglecting losses (h = ε= 0). The thermal power received by the active material is expressed by the relation:

$$P_t=\rho V C_p\frac{\Delta T}{\Delta t} \quad (14)$$

where:

ρ is Ni volume density, V the active material volume, and C_p, the thermal capacity.

4.2. Estimation of the Magnitude of the Different Thermal Losses

The transfer of kinetic energy from the active material (hot) to the wheel (cold) results in thermal loss by conduction, given by the equation:

$$P_{cond}=K*\frac{T_a-T_{Ni}}{L} \quad (15)$$

Additionally, the power lost by convection, with numerical application for half of the cycle $\frac{T_{Ni}}{2}$ and for $T_{Ni}=T_C$ (T_C being the Curie temperature of Ni, which is 631K), is expressed as follows:

$$P_{conv}=hS\left(T_{Ni}-T_a\right) \quad (16)$$

Radiation losses, presented for $\frac{T_{Ni}}{2}$ and for $T_{Ni}=T_C$, are expressed using the Stefan-Boltzmann law:

$$P_{rad}=\varepsilon S\sigma\left(T_{Ni}^4-T_a^4\right) \quad (17)$$

where S is the surface area, T_a is the ambient temperature, h, ε, and σ represent the heat transfer coefficient, the emissivity of the active material surface, and the Stefan-Boltzmann constant, respectively.

4.3. Estimation of the Characteristic Time During Heating

The characteristic time during heating can be estimate by the formula:

$$\tau=\frac{L^2}{D} \quad (18)$$

With D being the diffusivity of the active material, the characteristic time during heating can be given by

$$\tau=\rho C_p\frac{L^2}{D} \quad (19)$$

with L characteristic length and τ characteristic time

4.4. Estimation of the Cooling Time Constant

Knowing the thermal power concentrated by the solar collector on the active material, we can estimate the cooling time constant, using the relation:

$$P_t - \left(P_{cond} + P_{conv} + P_{rad}\right) = \rho V C_p \frac{\Delta T}{\Delta t} \quad (20)$$

Which is equivalent to:

$$\frac{\Delta T}{\Delta t} = \frac{P_t - \left(P_{cond} + P_{conv} + P_{rad}\right)}{\rho V C_p} \quad (21)$$

5. Results and Discussion

5.1. Magnetic Analysis

The maximum power of a thermomagnetic motor depends on the characteristics of the permanent magnet [19].

Table 1. Characteristics of Permanent Magnets

Type of Magnet	H_c(KA/m)	B_r (T)	$(BH)_{max}$ (kJ/m^3)
Nd-Fe-B	800-1200	1.2-1.4	600-800
Sm-Co	1200-1500	1.0-1.1	400-600
Fe-Co-Ni-Al	50-120	1.0-1.2	40-60
Fe-Cr-Co	40-70	1.3-1.6	40-60
Fe-Cr-Co	30-100	0.3-0.5	10-15

H_c is the coercive field, B_r is the remanent induction, and $(BH)_{max}$ is the volumetric energy density. This table shows that Nd-Fe-B present a more important volumetric energy density.

The selected Nd-Fe-B permanent magnets are of dimension (26 * 23 * 6.3) mm. These magnets will generate a magnetic field to attract the active material, with a Curie temperature T_C = 631K and dimensions of $10^{-2}*10^{-2}*10^{-3} m^3$. The objective of this section is to determine the attractive force.

Thus, for B_r = 1 T, x = 2*10^{-2}m, th_{PM} = 6.3*10^{-2}m, 2l = 26*10^{-2}m, and 2w = 23*10^{-2}m, we have a radiated field of $B_{PM}(x) = 0.2T$, using equation (1).

It is shown that parallelepiped magnets provide greater forces than cylindrical magnets of equivalent size [11]. Thus, in this section, we will consider a Neodymium-Iron-Bore (NdFeB) magnet exerting periodically an attractive and repulsive force on a Ni active material arranged on the lateral surface of the curie wheel.

For an active material with dimensions $10^{-2}*10^{-2}*10^{-3}$m^3, equation (6) gives $d(x) = d(y) = 0.2$ and $d(z) = 0.8$.

Hence,

$$\begin{cases} H_{total}(x) = H_{app}(x) - 0.2M(x) \\ H_{total}(y) = H_{app}(y) - 0.2M(y) \\ H_{total}(z) = H_{app}(z) - 0.8M(z) \end{cases} \quad (22)$$

Assuming the plate is magnetized along the x-axis, we have

$$M(x) = \frac{H_{app}(x) - H_{total}(x)}{0.2} \quad (23)$$

In the saturation regime, we have

$$\mu_0 M_{sat}(x) = 5^* \mu_0 H_{app}(x) = 0.94T \quad (24)$$

Therefore, the saturation field is 0.94T.

5.2. Thermal Loss Estimation

In this section, we will evaluate the order of magnitude of thermal losses and deduce the most effective ones for natural cooling.

For an average solar energy $E_{Sol} = 162*10^5$ J.m^2 [20,21], using a solar concentrator [22] collection surface $S_{col} = 900*10^{-3}$ J.m^2, the collector's energy is $E_{col} = 145.8*10^5$ J.

On the surface of the active $S_{AM} = 10^{-4} m^2$, the excitation energy $E_e = 1.6J$. During time $t_e = 1s$, we will have a power $P = 1.6W$.

The transmittance is given by the relation

$$\eta = \frac{P_e}{P_t} \quad (25)$$

For a transmittance of 92%, the excitation power is P_e = 1.49 W.

Now, we will estimate the expression of the temperature dependence over time, neglecting losses (h = ε = 0).

The thermal power received by the plate is expressed by the Equation (14), where ρ represents the volumetric density, V denotes the volume of the plate, given as $0.5*10^7$ m^3, C_p is the thermal capacity, and P_e is the excitation power.

Here, we assume that the active material is in contact with the wheel surface via a small cylinder of length and section s= a/10 (a being the side of the active material). We can notice that for $L = 10*10^{-3}$ m, we have $P_{cond} = 1.5W$ $T_{Ni} = 315.5K$ and 30.2 W at 631K.

As the convection, for $S = 10^{-4}$ m, we have $P_{conv} = 0.01W$ at $T_{Ni} = 315.5K$ and 0,8 W at 631 K

For the radiation, for $S = 10^{-4}$ m, we have $P_{rad} = 0.02W$ at $T_{Ni} = 315.5K$ and 0,33 W at 631K.

Concerning the axial characteristic time of thermal diffusion, we are at $0.5*10^{-3}$ m at 0,01s and $10^{-3} m$ at 0.04s.

It thus takes 10ms for the heat flux to travel 50% of the active material thickness.

For the lateral characteristic time, we are at $5*10^{-3}$m at 1.12s and $10^{-3} m$ at 4.49s

It then takes $1.2*10^3 ms$ for the heat flux to travel 50% of the active material width.

Consider an active material with volume V = $10^{-7}\,m$ in contact with the wheel via a small cylinder of section s= a/10 (a being the side of the active material) and length $L = 10*10^{-3}$ m. At T = T_C , we have $P_{cond} = 30.2W$, $P_{conv} = 0.33W$ and $P_{rad} = 0.8W$. This gives a loss P =31.1 W against Excitation Power P_e = $0.2*10^{-3}$ W.

$$\frac{\Delta T}{\Delta t} = -77K.s^{-1}$$

$$T_f = T_i + \left[-77(t_f - t_i)\right] \qquad (26)$$

where t_i is initial time (t = 0s), T_i is initial temperature T = 300 K.

Numerical operation gives 630.9K at $10^{-3}s$, 630.2 K at $10*10^{-3}s$ and 623.3 K at $100*10^{-3}s$.

This corresponds to a cooling percentage of 2.31% in 1 ms.

6. Conclusion

This article represents a significant advancement in our understanding of magnetostatic phenomena and thermal modelling within the context of Curie motor systems. By thoroughly investigating various intricacies, it sheds light on crucial aspects such as the intricate magnetic interactions between permanent magnets and active materials, the nuanced effects of demagnetizing fields, and the dynamic magnetic attraction forces at play.

Moreover, the study extends its scope to encompass the quantification of thermal losses occurring throughout rotation cycles. It meticulously evaluates the effectiveness of diverse cooling mechanisms in dissipating heat and preventing the accumulation of thermal energy within the active material. Additionally, by estimating characteristic time constants for thermal diffusion and cooling processes, the research provides valuable insights into the temporal dynamics of heat management within Curie motors.

Overall, this comprehensive analysis not only deepens our understanding of Curie motor dynamics but also paves the way for significant advancements in their optimization and practical implementation. As we continue to refine our understanding of these complex systems, we inch closer to realizing their full potential in various real-world applications, ranging from renewable energy generation to advanced robotics and beyond.

References

[1] Karle, A., "The thermomagnetic Curie-motor for the conversion of heat into mechanical energy," *International Journal of Thermal Sciences*, 40(9), 2001, 834-842.

[2] Vuarnoz, D., Kitanovski, A., Gonin., C., Borgeaud, Y., Delessert, M., Meinen, M. and Egolf, P.W., "Quantitative feasibility study of magnetocaloric energy conversion utilizing industrial waste heat," *Applied Energy*, 100, 2012, 229-237.

[3] Christiaanse, T., and B., Ekkes, "Proof-of-concept static thermomagnetic generator experimental device", *Metallurgical and Materials Transactions E*, 1, 2014, 36-40.

[4] Trapanese, M., "A dq axis theory of the magnetic, thermal, and mechanical properties of curie motor," *Journal of Applied Physics*, 109(7), 2011, 07E706.

[5] Alves, C., Colman,F., Foleiss, G., Szpak, W., Vieira, G., and Bento, A., "Simulation of solar curie wheel using NiFe alloy and Gd, " *International Journal of Refrigeration*, 37, 215– 222, 2014.

[6] Afenyiveh, S. D. M., Adanlété Adjanoh, A., Douti, D. L., and Pakam, T., "Thermal simulation and optimization of a Curie-based thermomagnetic motor harnessing concentrated solar energy". *AIP Advances*, 14(2), 2024, 025221.

[7] Akoun; G., and Yonnet, J.P., "3d analytical calculation of the forces exerted between two cuboidal magnets," *Magnetics, IEEE Transactions on*, 20(10), 1984, 1962–1964.

[8] Nguyen, T and Lu, T. F., "Analytical expression of the magnetic field created by a permanent magnet with diametrical magnetization," *Progress In Electromagnetics Research C*, 2018, 87(10).

[9] Bekinal,S., and Jana, S., "Analysis of the magnetic field created by permanent magnet rings in permanent magnet bearings," *International Journal of Applied Electroma gnetics and Mechanics*, 46(06), 2014, 255–269.

[10] Fortkamp, F., Lozano, J., and Barbosa, J., "Analytical solutions of the magnetic field generated by two-pole nested Halbach cylinders," 09 2016.

[11] Agashe, J. S. "A study of scaling and geometry effects on the forces between cuboidal and cylindrical magnets using analytical force solutions", *Journal of Physics D: Applied Physics*, 41, 2008, 105001.

[12] Furlani, E. P., "Permanent magnet and electromechanical devices: materials, analysis, and applications", *Academic Press*, 2001.

[13] Homadi, A., and Hall, T., "Enhancement the Frequency of a New Oscillating Thermomagnetic Generator", *2019 IEEE Texas Power and Energy Conference (TPEC).*

[14] Forrer, R., Martak, J., "Le champ démagnétisant structural des ferromagnétiques et sa détermination expérimentale", J. Phys. Radium, 2 (6), 1931, 198-204.

[15] Joseph, R. I., and Schlömann, E., "Demagnetizing Field in Nonellipsoidal Bodies", *Journal of Applied Physics*, 36, 1965, 1579.

[16] Zheng, G., Pardavi-Horvath, M., Pardavi-Horvath, X. Huang, Huang, X., Keszei, B., and Vandlik, J., "Experimental determination of an effective demagnetization factor for nonellipsoidal geometries", *Journal of Applied Physics*, 79, 1996, 5742-5744.

[17] Aharoni, A., Demagnetizing factors for rectangular ferromagnetic prisms, *Journal of Applied Physics*, 3, 1998, 3432.

[18] Zhang, J., Li, M., and Morimoto, K., "Sintering of solution-based nano-particles by a UV laser pulse train", *Proceedings of SPIE - The International Society for Optical Engineering*, 7920(2), 2011.

[19] Elliott, J. F., "Thermomagnetic Generator", *Journal of Applied Physics*, 30, 1959, 1774–1777.

[20] Afenyiveh, S. D. M., Kodjo, K. M., and Hova, H., "Static evaluation of the global solar potential in the region of Kara (Togo) by empirical models," *International Journal of Advanced Research* 7, 2019; 830–835.

[21] Afenyiveh, S. D. M., Kodjo, K. M., and Hova, H., "Dynamic evaluation of global solar potential in the region of Kara (Togo) by artificial neural network," *International Journal of Engineering Sciences & Research Technology* 8, 2021, 193-202.

[22] Afenyiveh, S. D. M., Adanlété Adjanoh, A., and Douti , D. L., "Optical simulation of a parabolic solar concentrator," in Conference Proceedings: 1st German-West African Conference on Sustainable, Renewable Energy Systems SusRes: 1st July 2020-Kara, Togo 2020, 66–72.